International Journal of Theoretical Physics, Vol. 43, No. 3, March 2004 (© 2004)

Cosmic Microwave Background and Inflation Parameters

J. Richard Bond,[1,3] Carlo Contaldi,[1] Antony Lewis,[1] and Dmitry Pogosyan[2]

We review the current cosmic parameter determinations of relevance to inflation using the WMAP-1 year, Boomerang, CBI, Acbar, and other CMB data. The basic steps in the pipelines which determine the bandpowers from the raw data from which these estimations are made are summarized. We forecast how the precision is likely to improve with more years of WMAP in combination with future ground-based experiments and with Planck. We address whether the current data indicates strong breaking from uniform acceleration through the relatively small region of the inflaton potential that the CMB probes, manifest in the much-discussed running spectral index or in even more radical braking/breaking scenarios. Although some weak "anomalies" appear in the current data, the statistical case is not there. However increased precision, at the high multipole end and with polarization measurements, will significantly curtail current freedom.

KEY WORDS: early universe; inflation; CMB.

1. INTRODUCTION TO CMB POWER SPECTRA

1.1. Overview

The three Peyresq lectures covered CMB theory and analysis. The main content and most of the relevant references are given in Bond *et al*. (2003, hereafter BCP). Although a summary of that material will be given here, in this paper we will emphasize the impact on inflation phenomenology of the experiments WMAP, Boomerang, CBI, and Acbar, in conjunction with DASI, VSA, Archeops, Maxima, TOCO, earlier CMB experiments, and with large-scale structure (LSS) observations. We will also remind the reader of the great success now of CMB determinations of the material content of the universe, including

[1] CIAR Cosmology & Gravity Program, Canadian Institute for Theoretical Astrophysics, Toronto, Ontario, Canada.
[2] Physics Department, University of Alberta, Edmonton, Alberta, Canada.
[3] To whom correspondence should be addressed at CIAR Cosmology & Gravity Program, Canadian Institute for Theoretical Astrophysics, Toronto, Ontario, Canada; e-mail: bond@cita.utoronto.ca.

0020-7748/04/0300-0599/0

dark energy and dark matter. A detailed treatment of LSS and the relation to the Sunyaev–Zeldovich (SZ) effect, the cluster-dominated upscattering of CMB photons from hot electrons in the cosmic web, was covered in the third lecture, and in Bond *et al.* (in press) and Readhead *et al.* (2004) (see also Bond and Crittenden, 2001). At Peyresq, Page looked to the future with WMAP and the Atacama Cosmology Telescope (ACT) and de Bernardis covered Boomerang and beyond, concentrating on polarization. We will also explore here how such future CMB observations may help to further discriminate among inflation models.

The theory of Gaussian primary anisotropies, those arising from linear physics operating in the early Universe, is in good shape. For the current data, speedy codes efficiently using past-history integrations such as CMBfast and CAMB are quite adequate, and have been "validated" with codes solving hierarchies of multipole equations. As precision in the data improves, fresh looks at all aspects of the accuracy are worthwhile, and are being done.

For secondary anistropies, those arising once nonlinearity develops, the computational state of the art continues to need much further effort. This includes the important component which rears its head at small angular scales associated with the SZ effect. The statistically inhomogeneous Galactic foregrounds offer even more of a theoretical challenge, and this has only partly been addressed. The direct interface with observations for these many non-Gaussian signals is much more complex than for Gaussian primary anistropies. Because all the signals are superimposed. the separation of the primary, secondary, foreground, and extragalactic components inevitably complicates the move from multifrequency CMB data to determination of cosmic parameters from "cleaned" primary CMB power spectra.

Major efforts by many groups around the world have been put into developing the statistical pipelines which process and clean the raw CMB data to allow efficient and accurate confrontation with the theory. Even if primary power spectra are the primary target to be extracted from the data, the case so far, the sophistication level required is high: processing timestreams or interferometer visibilities, making maps in position or "momentum" space, filtering, cleaning, separating component signals, compressing, always with new tools to explore systematic effects and anomalies that inevitably appear. The step from raw data to primary power spectrum is enormous, from power spectrum to parameters small. Most of the developments were driven by the compelling necessity of the CMB teams, consisting of theorists/analysts as well as experimentalists, to extract accurate science from beautiful large datasets such as Boomerang and CBI, yet remain within computational feasibility. Polarization analysis is receiving much further attention now, and in spite of the many algorithmic advances in the analysis pipeline in recent years, many more are needed for the rosy forecasts of high precision described here to be realized.

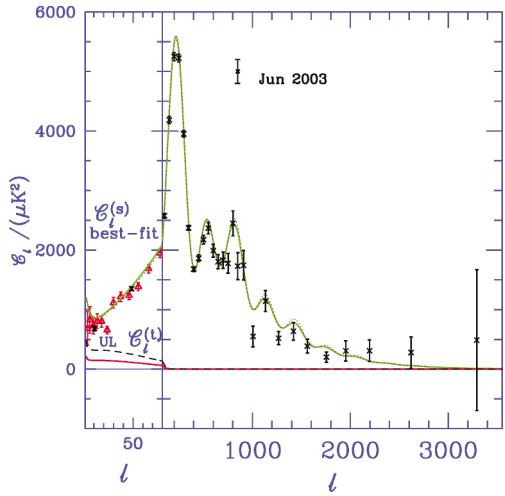

Fig. 1. An optimal Grand Unified Spectrum for the post-WMAP Jun03 data is shown as crosses. This GUS is a maximum-likelihood determination of the power in 26 (top-hat) bands, with calibration and beam uncertainties of the various experiments fully taken into account. A best-fit inflation-based uniform-acceleration ACDM $\mathcal{C}_\ell$ spectrum to this Jun03 data is shown as solid green. The parameters are $\{\Omega_{\rm tot}, \Omega_\Lambda, \Omega_{\rm b}h^2, \Omega_{\rm cdm}h^2, n_{\rm s}, \tau_{\rm C}, t_0, h, \sigma_8\} = \{1.0, 0.712, 0.0224, 0.118, 0.957, 0.108, 13.7, 0.698, 0.84\}$. The WMAP1 data optimally compressed on to 49 bandpowers is also shown for low ℓ as triangles in the lower ℓ part of the figure, to highlight the two low-ℓ "anomalies," at ℓ of a few and at $\ell \sim 20$. The best-fit $\mathcal{C}_\ell$ would fit better with a slight downward tilt below $\ell \sim 30$ and beyond $\ell \sim 500$, which a scale-dependent $n_{\rm s}(k)$ could do (§II). Peak and dip locations derived from this optimal spectrum are shown in Fig. 2.

1.2. Grand Unified Spectra of CMB Data

Figure 1 shows a "Grand Unified Spectrum" $\mathcal{C}_\ell$ as a function of multipole ℓ compressed on to a small number of bandpowers, derived from a June 2003 compilation of CMB data. A best-fit inflation-based uniform-acceleration model to that data is also shown. In place of determining "cosmological parameters" from the observed bandpowers for various experiments, the parameters here are in fact power amplitudes in multipole bands chosen by the analyst. Oher parameters characterizing experimental uncertainties in calibration and beams are also determined simultaneously. In determining errors on the cosmological parameters and/or the

GUS bandpowers, the other variables are marginalized (probability distributions are integrated).

To see the remarkable evolution that has occured in $\mathcal{C}_\ell$ in just a few years we refer the reader to Fig. 1 of BCP. This shows a sequence of four GUS derived for the data extant in Jan00, Jan02, Jun02,and Jan03. (For experimental acronyms and much more detailed discussion of how the results from the different experiments were used see BCP.) The GUS are in excellent agreement with each other and with the first-year WMAP results, hereafter WMAP1. All pre-WMAP1 CMB results relied heavily on COBE's DMR results, which anchored the low $\ell \lesssim 30$ multipoles. Fortunately WMAP1 spectacularly confirmed DMR. Jan00 included TOCO and the Boomerang North America test flight, as well as 19 previous experiments, including upper limits. Jan02 included Boomerang, DASI, and Maxima as well. Jun02 had CBI and VSA added as well. By Jan03, improved Boomerang results were added to preliminary 2-year CBI results, extended VSA results, Acbar, and Archeops.

By Mar03, the WMAP1 data were incorporated, and recalibrated CBI 2 year and VSA results were included. The recalibration was tiny but the errors on the calibration decreased by a factor of 2. The latter was done off WMAP1, using observations of Jupiter. In GUS methods the relative calibrations and their errors come out as a byproduct. BCP showed these were in excellent agreement with cross-comparisons made by Eric Hivon between WMAP1 and Boomerang maps, and with the CBI calibration using WMAP1. A Jun03 compilation utilized GUS-based recalibrations of Boomerang and of ACBAR. The Jun03 GUS shown in Fig. 1 differs only slightly from the Mar03 GUS used in BCP. This is basically because experimental calibrations and beam sizes are internally determined and marginalized over in making the GUS: if the method is correct it will give robust results—and it does. The CBI 2-year data has now been released Readhead *et al*. (2004). The Jun03 GUS in Fig. 1 does not include the new VSA data (Dickinson *et al*., 2004), but it has little effect on the spectrum, and on cosmological parameter determinations.

WMAP1 dominates the $\ell \lesssim 600$ bands. Unless explicit joint analyses are done of experiments with significant overlap with WMAP's all-sky coverage, the band-powers for such experments should be dropped from the GUS and parameter determinations. Thus COBE and Archeops were not included in the Mar03 and Jun03 compilations.

1.3. Peaks, Dips, and Damping

Figure 2 illustrates some of the "pillars" that we were looking for in the TT data to verify the paradigm, exemplified by the best-fit power-law model. (1) The effects of a large-scale gravitational potential at low multipoles, manifested by a "Sachs-Wolfe" plateau; note the integrated SW upturn associated with Ω_Λ driving

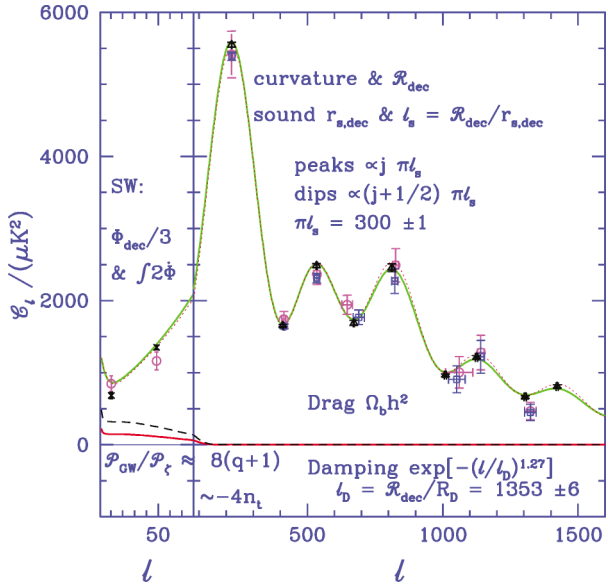

Fig. 2. Various pillars which determine the inflation-based uniform-acceleration $\mathcal{C}_\ell$ spectrum shown that best-fits the Jun03 data are highlighted. The low ℓ part of the figure repeats as crosses the two Jun03 bands of Fig. 1 and contrasts these with the equivalent two bands for the pre-WMAP1 Jan03 data, which includes COBE and Archeops. The low ℓ shape arises both from the climb of the photons through the potential well at decoupling and the propagation of the photons through a time varying gravitational potential along the line of sight. Also shown at the bottom is the expected tensor component for uniform acceleration with tensor tilt $n_t = n_s - 1 = -0.043$, and above it the Spergel *et al.* (2003) 95% CL limit, corresponding to $\mathcal{P}_{GW}/\mathcal{P}_\zeta < 0.36$. The higher ℓ part of the figure shows the peak/dip locations $\ell_{pk/dip,j}$ and heights $\mathcal{C}_{pk/dip,j}$, as determined from the BCP maximum-likelihood-sliding-band approach. The points with slightly larger errors are for the pre-WMAP1 Jan03 data and the heavier are for the post-WMAP1 Jun03 data. The triangles show the values obtained by ensemble-averaging peak/dip locations and heights over the large $\mathcal{C}_\ell$-database used in BCP. (Only a weak prior was applied, which allows large movement of peak locations associated with the geometry, hence is preferable to more restrictive priors for this application. Note how well these statistically-averaged peaks and dips match those of the best-fit model.)

a time-varying gravitational potential at low ℓ and the upturn at higher ℓ associated with photon compressions and rarefactions.

At higher ℓ the next pillars are (2) the pattern of acoustic peaks and dips and (3) the damping tail. These are governed by the comoving sound speed $r_s =$

146 ± 3 Mpc and damping length $R_{\rm D} = 10.3 \pm 0.21$ Mpc at photon decoupling, and are scaled with the angular–diameter distance relation $\mathcal{R}_{\rm dec}$ to decoupling to get the associated $\ell_{\rm s}$ and $\ell_{\rm D}$ values which define the peak/dip and damping structure.

Figure 2 shows the peak/dip locations and amplitudes and their one-sigma error bars, as determined in BCP, contrasting Jan03 with Jun03. The exercise in BCP was to do this directly from the relatively broad-band GUS, using a model that slides a sequence of bands across the data sets. In spite of the coarseness of the bands, the peak/dip results are highly accurate as long as all band-to-band correlations are taken into account. These peak and dip parameters have also been determined for individual experiments such as TOCO, Boomerang, CBI, Archeops, and of course for WMAP1, the latter described in Page *et al*. (2003). Values are given in BCP, Table 2

There is good evidence from WMAP1, Boomerang and other CMB analyses that the statistics of the primary anisotropies are predominantly (4) Gaussian, i.e., have maximal randomness for a given power spectrum. Finding (5) secondary anisotropies associated with nonlinear phenomena, due to the SZ thermal and kinetic effects, inhomogeneous reionization, weak lensing, etc. is expected. The anomalous extra power at high ℓ over the best-fit primary model evident in Fig. 1 arises from combining CBI and Acbar data. Assuming an SZ spectrum makes the case somewhat stronger, and suggests this pillar may have been seen (see Fig. 8 and Bond *et al*., in press; Goldstein *et al*., 2003; Readhead *et al*., 2004).

(6) Polarization must be there, with forecasted $C_\ell^{\rm (EE)}$-patterns of peaks and dips intimately related to, though with different phases than, those for TT. As well there is a specific peak/dip pattern in the TE cross-correlation of the E-mode with the total intensity predicted. The current status of polarization is a broad-band EE detection consistent with inflation by DASI and of course the remarkable TE cross correlation of WMAP1. More EE detections are expected soon from WMAP2, CBI, and Boomerang, and there are many planned experiments that should exquisitely determine the EE and TE spectra. Figures 3, 4 and 5 show the TE and EE spectra for the best-fit model and forecasts of polarization detections by WMAP4, by Planck1, and by a fiducial ground-based large-array polarization-sensitive telescope.

A future goal for CMB researchers is to find (7) the anisotropies induced by gravity wave quantum noise. Not all inflation models predict this, but the well known simple relation between tensor tilt $n_{\rm t}$ the deceleration parameter q and the tensor-to-scalar power ratio shown in Fig. 2 suggests there may be a strong enough signal to detect. For the Jun03 best-fit model shown with scalar index $n_{\rm s} = 0.957$, a uniform acceleration model yields a tensor-to-scalar contribution of 0.17 cf. the Spergel *et al*. (2003) upper limit of 0.36 at the 95% CL. A holy grail for the subject is to detect the B-mode of polarization at low ℓ. For these best-fit parameters, it may be do-able with the Planck satellite as the lower panel of Fig. 4 illustrates. A nice figure summarizing EE and BB bandpower forecasts for various experiments such as QUaD and BICEP in comparison with Planck is given in Hivon and Kamionkowski (2002).

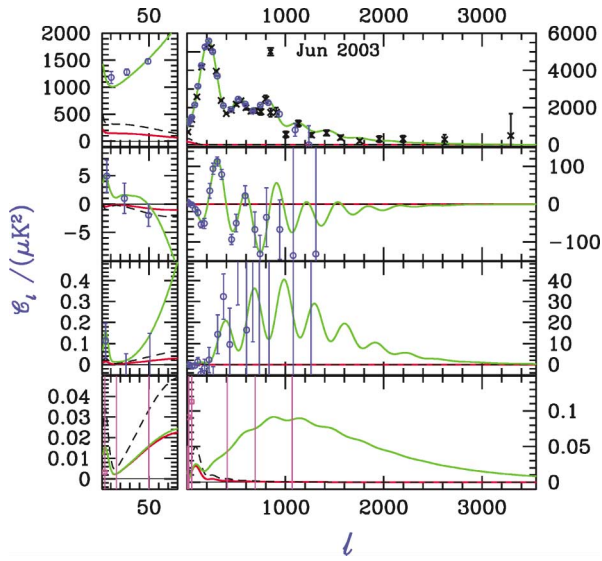

Fig. 3. Idealized forecasts for detections of (top to bottom) TT, TE, EE, and BB bandpowers by WMAP with 4 years of 94 GHz channel data. This is a conservative estimate given the other WMAP frequencies, but idealized in the sense that foregrounds and other experimental complications are ignored. Simulations use the best-fit Jun03 model (shown). The Jun03 GUS are the crosses in the TT panel. Note the very different scales on the low and high ℓ panels of the figure. As well as the target scalar $\mathcal{C}_\ell^{(s)}$, the tensor $\mathcal{C}_\ell^{(t)}$ contributing at the level predicted if $n_t = n_s - 1$ is also shown. The tensor shape is repeated with the amplitude corresponding to the current WMAP1 upper limit on the tensor to scalar ratio. Only the B-mode from primary tensor anisotropies is shown. Primary scalar perturbations have no B-mode in linear perturbation theory, but they are induced by lensing (Hu, 2000). These and the unknown foregrounds present severe challenges for confirmation of the gravity-wave-induced B-mode. The B-mode bandpower spacings differ from the spacings used for the upper panels.

The very tiny B-mode signal predicted and the unknown nature of the polarized foregrounds would make this a very hard task indeed, one happily defining a long-term future for CMB research as the community plans a future NASA CMBPol satellite as the next step in space after Planck.

2. COSMIC PARAMETERS AND INFLATION ISSUES

2.1. The Conventional Minimal Parameters

To the well known minimal inflation-motivated set, $\{\Omega_b h^2, \Omega_{cdm} h^2, \Omega_k, \Omega_\Lambda, n_s, \tau_C, A_s\}$, defining the allowed C_ℓ shapes. other parameters are sequentially added

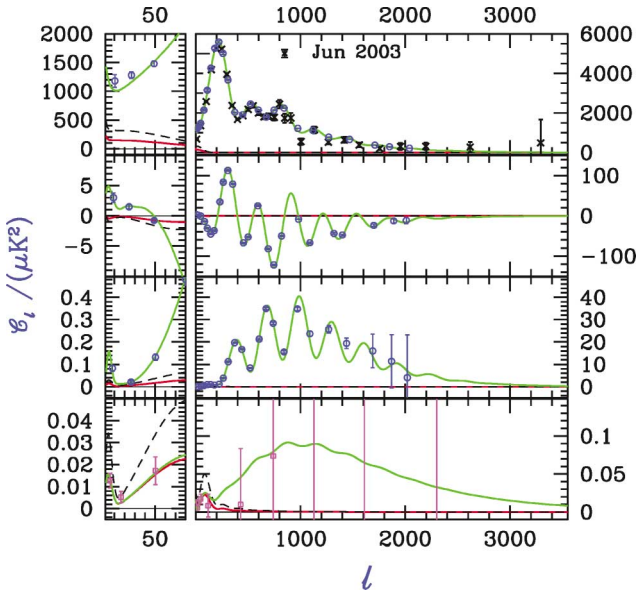

Fig. 4. Forecast for how well Planck can do with just its 150 GHz channels for 1 year of data, quite a conservative estimate. Even so, note the anticipated detection level of EE and TE at low ℓ, sharpening the τ_C determination, and the possibility of a statistically significant direct tensor-induced B-mode detection. Although ground-based experiments at high resolution should have a huge pre-Planck impact (e.g., Fig. 5), the all-sky nature of Planck, its large set of polarization-sensitive frequencies and its longer observing time than that assumed will make it extremely powerful to sort out the many signals that complicate the "primary" quest.

to probe more complex models of inflation or of matter content. (Ω_j is the density parameter ρ_j relative to the critical density $\rho_{cr} = 10.5\,h^2$ kev cm^{-3}, where h is the Hubble parameter in units of 100 km s^{-1} Mpc^{-1}, so $\Omega_b h^2$ and $\Omega_{cdm} h^2$ are proportional to the physically more relevant baryon and cold dark matter densities.) The vacuum energy is Ω_Λ and the mean curvature energy for our Hubble patch is Ω_k in terms of which the total energy content is $\Omega_{tot} = 1 - \Omega_k$. Sample content extras include a subdominant light neutrino component, enhanced relativistic particles $\Omega_{er} h^2$, e.g., as products of decay of massive particles, adding dynamics to Ω_Λ, e.g., through a parameterized time-dependent pressure-to-density ratio, $w_\Lambda(t)$.

Astrophysical complications associated with the "late time" impact of reionization of the Universe, presumably by the injection of energy from the first stars, are encoded in a single parameter τ_C, the depth to Compton scattering when the Universe reionized. τ_C could have a complex temporal and spatial structure, and,

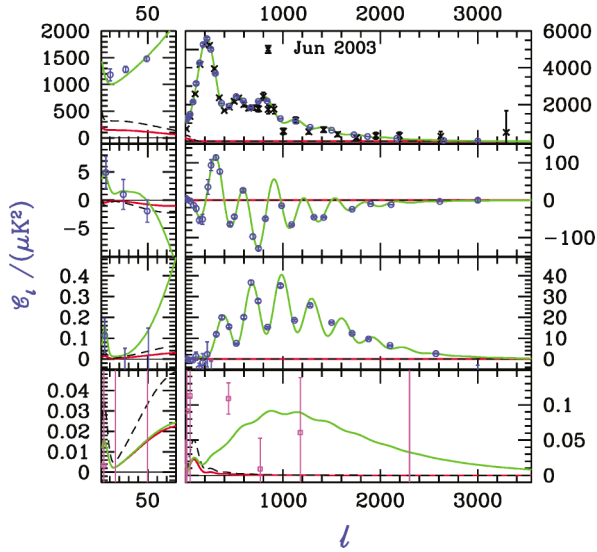

Fig. 5. Forecast for how well a high-resolution ground-based polarization-sensitive large-array experiment like ACT or SPT can do, in conjunction with WMAP4. The specific assumptions used are given in the caption of Fig. 10 and are conservative over what might be achievable from the ground using bolometer arrays. Apart from the current DASI, WMAP, Boomerang, and CBI data already in to flesh out the EE spectrum, a number of other experiments are planned. These include some in the very near future, e.g., QUaD and BICEP. Forecasts for the proposed QUIET with HEMT arrays look as promising as those for ACT/SPT. Given the expected signal levels, all ground and space CMB information available will be needed and used to get clean primary polarization results.

although the CMB primary anisotropies are not that sensitive to the details, finding such signatures in the data is a target of planned high resolution experiments.

2.2. The Inflation Parameters

Inflation fluctuations are assumed to have a Gaussian statistical distribution, fully specified by a power spectrum of curvature perturbations $\mathcal{P}_{\varphi_{\rm com}}(k)$. The minimal set has only two parameters, the overall initial power spectrum amplitude $A_{\rm s} \equiv \mathcal{P}_{\varphi_{\rm com}}(k_n)$, evaluated at a normalization wavenumber $k_{\rm n}$, and a single spectral scalar index $n_{\rm s}(k) = n_{\rm s}(k_n)$.

There is of course a vast literature on perturbation theory as applied to inflation (e.g., Bond 1994, 1996 for the approach described here). Basic variables are

the inflaton field $\delta\phi_{\rm inf}$: other scalar field degrees of freedom $\delta\phi_{\rm is}$ which can induce scalar isocurvature perturbations; two gravitational wave polarization modes $h_+, h_\times$. One can encode scalar metric perturbations and their variations through the inhomogeneous scale factor $a(\mathrm{x}, t)$, Hubble parameter $H(\mathrm{x}, t)$ and deceleration parameter $q(\mathrm{x}, t) \equiv -d\ln Ha/d\ln a$. For example, the scalar 3-curvature is $-4\nabla^2 \ln a$. Inflation ends when q passes from negative to positive.

Certain time hypersurface upon which to measure the perturbations simplify things quite a bit. Sample choices are $\phi_{\rm inf}$, $\ln a$, $\ln H$, $\ln(Ha)$, and conformal time $\tau = \int d\ln a/(Ha)$. The power spectrum $\mathcal{P}_{\ln a|_{H_*}}(k)$ of scale factor fluctuations evaluated on time hypersurfaces on which the Hubble parameter H is constant becomes time-invariant for wavenumbers $k/Ha \ll 1$ (outside of the "horizon"), if there is just one dynamically important scalar field, and remains so until fluctutions regain causal contact. If the universe has no net mean curvature, $\varphi_{\rm com} = \delta\ln a|_{H_*}$, measuring the curvature on comoving hypersurfaces. Another variable used extensively is ζ, which reduces to $\varphi_{\rm com}$ if $k/Ha \ll 1$, hence we sometimes refer to $\mathcal{P}_\zeta$ in the figures.

The gravity wave power $\mathcal{P}_{\rm GW}(k) \equiv (k^3/2\pi^2)\langle h_+^2 + h_\times^2\rangle = (k^3/2\pi^2)\langle h_{\rm ij}h^{\rm ij}\rangle/2$ used here and in Bond (1994, 1996) is defined to be consistent with the conventions of GW detection research, with GW mode functions being the usual $h_\times = h_{12} = h_{21}$, $h_+ = (h_{11} - h_{22})/2$. Most people in inflation define a $\mathcal{P}_h(k) = 2\mathcal{P}_{\rm GW}(k)$, which is what $A_{\rm t} \equiv \mathcal{P}_h(k_n)$ is defined to be.

Quantum fluctuations in gravity waves must occur during inflation. The only question is how $\mathcal{P}_{\rm GW}$ compares with $\mathcal{P}_{\varphi_{\rm com}}(k_n)$. Thus the minimal $A_{\rm s}$, $n_{\rm s}$ should at the very least be augmented by an $A_{\rm t}$ and $n_{\rm t}$. As well subdominant isocurvature components can be added, $A_{\rm is}$ and $n_{\rm is}$.

For all of these cases, "radically broken scale invariance" may prevail, in which the spectral index functions

$$n_{\rm s}(k) - 1 \equiv d\ln\mathcal{P}_{\varphi_{\rm com}}(k)/d\ln k = 2(1+q^{-1}) + q^{-1}q'/(1+q) + 2C_{\rm s}, \quad (2.1)$$

$$q' = dq/d\ln a = -q\,dq/d\ln(Ha),$$

$$n_t(k) \equiv d\ln\mathcal{P}_{\rm GW}(k)/d\ln k = 2(1+q^{-1}) + 2C_{\rm t}, \quad (2.2)$$

can be relatively arbitrary functions of spatial wavenumber rather than constants. Here quantities such as q and q' are evaluated at the "time" $Ha = k$. The formula is motivated by the stochastic treatment of inflation in the Hamilton Jacobi framework, in which quantum noise at the Hawking temperature $H/2\pi$ radiates from short distances across the decreasing $(Ha)^{-1}$ boundary into a long wavelength background field. The postinflation power spectra are parameterized by

$$\mathcal{P}_{\ln a|_{H_*}} = \frac{1}{q+1}\frac{4\pi}{M_{\rm P1}^2}(H/2\pi)^2\, e^{2u_{\rm s}}, \quad \mathcal{P}_{\rm GW} = 8\frac{4\pi}{M_{\rm P1}^2}(H/2\pi)^2\, e^{2u_{\rm t}}. \quad (2.3)$$

Of course the utility of these expressions depends upon the correction factors $C_{\rm s,t}$, which are derived from the related $u_{\rm s,t}$. Analytical forms for special cases can be derived, e.g., for uniform acceleration, and these show the $C_{\rm s,t}$ are typically small.[4] Much has been written on this subject. See, for example, Bond (1994), Lidsey *et al.* (1997), Wang *et al.* (1997), Schwarz *et al.* (2001), Kinney (2002), Habib *et al.* (2002), Martin and Schwarz (2003), Peiris *et al.* (2003), Leach and Liddle (2003), and references therein. The accurate path to the spectral indices is to take logarithmic derivatives of full numerical calculations to get the $C_{\rm s,t}$. One can certainly invent cases in which the $C_{\rm s,t}$ are not small. However, provided q does not change too rapidly it is reasonable to use these formulas as guides. They show that tilt mostly depends upon how far the acceleration is below the *critical* value of unity. For $q \approx -1$. a substantial scalar tilt can come from the second term, yet no tensor tilt, as in natural inflation.

Deviations from the power law model are not just expected, they are necessary, since $q(k)$ must have passed from negative to positive to have created matter from the vacuum energy housed in the inflaton. The simplest form of braking of the acceleration is the running index, $n_{\rm s}(k) = n_{\rm s}(k_n) + [dn_{\rm s}/d\ln k(k_n)]\ln(k/_{kn})$. Such a form can be expressed in terms of coefficients q_n, q'_n, q''_n in an expansion of $q(k)$.

A priori, it may seem unlikely that a marked change in the expansion rate or acceleration would just happen to be in the three-decade window of k-space accessible to our CMB observations, since it maps into a relatively small patch on the inflaton potential surface because of the $(1+q)$ suppression factor in $\frac{\sqrt{4\pi}}{M_{\rm Pl}}\,d\phi = \pm q^{-1}\cdot(1+q)^{1/2}d\ln(Ha)$. That is that q'_n would be small. However in ϕ-space, this CMB window is not very far from $\phi_{\rm end}$ defining the acceleration/deceleration boundary, hence the q rise to zero must be reasonably rapid in ϕ. Even so, for most inflation models, the rapid change does indeed occur only near the end, suggesting special physics might have to be built in to accommodate large change. Rapid acceleration changes, if present, would seem to be more likely a consequence of interaction with other field degrees of freedom rather than a result of inflaton self-interaction. Such hybrids involving two scalars interacting with either simple polynomial potentials (with second-, third-, and fourth-order terms), combinations of exponential potentials, and other simple forms, have long been used to show that constructing power spectra with mountains and valleys and even generating non-Gaussian fluctuations is possible in inflation.

[4] The stochastic inflation technique uses "the $H/(2\pi)$ at $k = Ha$ WKB approximation," writes Eq. (2.3) as a function of H, q, and derivatives, and takes a logarithmic derivative wrt Ha in place of k. Analytical corrections invariably involve Hankel functions and their asymptotic expansions. No slow roll ($(1+q)\approx 0$) restrictions are needed in these approaches. In the HJ formulation, (Salopek and Bond, 1990, 1991) $H(\phi)$ and $q(\phi)$ are treated as functions of the inflaton field, and satisfy the "reduced Hamilton–Jacobi equation" relating $H(\phi)$ to the potential $V(\phi)$: $H^2_{\rm SR}/(1-(q+1)/3)$, where $H^2_{\rm SR} \equiv \frac{8\pi V}{3M^2_{\rm Pl}}$ and $(1+q) = \frac{M^2_{\rm Pl}}{4\pi}[\frac{\partial \ln H}{\partial\phi}]^2$. The extra piece in $n_{\rm s} - n_{\rm t}$ is $q^{-1}q'/(1+q) = -q^{-1}\frac{M^2_{\rm Pl}}{4\pi}\frac{\partial^2 \ln H}{\partial\phi^2}$, responsible for deviations in the two indices that can be signficant near $(1+q)\approx 0$.

However even if more than one scalar field enters it is often possible to consider an effective single inflaton self-interacting through an effective single-inflaton potential over the observable scales. This is because the fields first settle into gorges on the potential surface, then follow the gorge downward toward the local minimum along a single-field degree of freedom, $\phi_\parallel$, to be identified with the inflaton. The other degrees of freedom, $\vec{\phi}_\perp$, are "isocurvature" degrees of freedom. Usually, the faces rising up from the gorge will be sufficiently steep that the inevitable quantum noise that excites motion up the walls quickly falls back, leaving no usable isocurvature imprint, effectively making those dimensions irrelevant (although curvature in the trough can lead to complications in the kinetic energy piece of the inflaton degree of freedom). The single-inflaton expressions in terms of q would prevail.

To get observable response often involves invoking an instability, with negative transverse components of the mass-squared matrix, $\partial^2 V/\partial\phi_i\,\partial\phi_j$, leading to an opening up of the gorge or its bifurcation. Tuning the location of such a structure to the window on the potential surface we can access may seem to be unpalatably precise. This is perhaps mitigated by relating it to a waterfall of sudden q change to trigger reheating, termed hybrid inflation. Control of residual defects left from the potential was always an issue, though such residual subdominant components are worthwhile to hunt for in the data. Although these multiple-field models would have significant deceleration occurring in a waterfall phase, to have a spectrum with many sharp features littering the CMB range parameterizing a complex braking pattern seems very baroque indeed. (These multiple-field situations are the ones where the simple spectral index formulas in terms of q are likely to have the largest corrections.) CMB phenomenologists should constrain such possibilities anyway. We shall see that the prognosis for constraining even such radical braking is reasonable with upcoming CMB experiments.

The richness of inflation theory has expanded considerably with the emphasis on higher dimensions, brane-ology, and stringy cosmology. So far to the extent there are predictions they fit within the basic inflation phenomenology as applied to CMB analysis of the sort described here. It would be nice if a smoking gun pointing to a uniquely stringy culprit will be found theoretically, and in the data.

3. PARAMETER ESTIMATIONS, NOW AND FUTURE

3.1. Parameters From the Jun03 Data

Figure 6 shows visually the one- and two-sigma constraints for the minimal inflation parameter set derived from the Jun03 CMB dataset using the Monte Carlo Markov Chain method. These results were also reported in Readhead *et al.* (2004) and are very similar to the Mar03 results given in BCP. BCP showed that the MCMC results were also in good agreement with those obtained using fixed

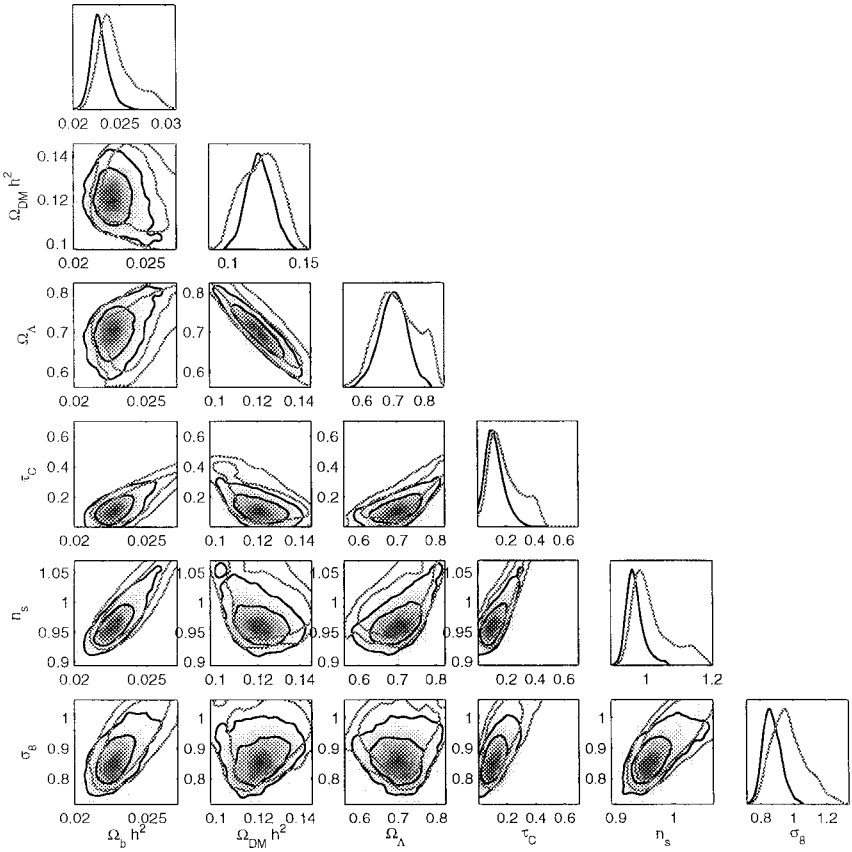

Fig. 6. The state of parameter estimation using the Jun03 data compilation is illustrated by the one and two sigma contour regions when all but the two variables shown are marginalized. The scalar spectral index was not allowed to run. The outer contours are for WMAP1 alone. The 1-D probability distributions for each single variable shown at right gives means and 1-sigma errors listed in Table I. This illustrates how the current data to higher ℓ, predominantly driven by Boomerang, CBI, and Acbar, sharpen the WMAP1 results by breaking partial degeneracies. The priors applied were $\Omega_k = 0$ and the weak h-prior. In the figures, the σ_8-dominated LSS prior was included as well. The table shows the extent to which this sharpens parameter determinations.

$\mathcal{C}_\ell$-grids. Table I gives projected one-sigma MCMC errors. Priors applied to augment the CMB data with other information range from weak ones to stronger constraints from the expansion rate (HST-h), from cosmic acceleration from supernovae (SN 1) and from galaxy clustering, gravitational lensing, and local cluster abundance (LSS). We show results in the table for CMB + weak and CMB + weak + LSS, with a flat $\Omega_{\rm tot} = 1$ prior also imposed.

Table I. Sample Cosmological Parameter Values and Their One-Sigma Errors Determined by Using MCMC Methods After Marginalizing Over the Other Cosmological Parameters and for Real data, the Various Experimental Parameters

MCMC	WMAP1	Jun03	Jun03 + LSS	Jun03 + 2dF	WMAP4	Planck1
Flat + Weak						
$\Omega_b h^2$	0.0243 ± 0.0018	0.0228 ± 0.00095	0.0229 ± 0.00097	0.0228 ± 0.00090	0.02271 ± 0.00047	0.02256 ± 0.00017
$\Omega_{cdm} h^2$	0.123 ± 0.018	0.118 ± 0.011	0.121 ± 0.009	0.120 ± 0.007	0.1122 ± 0.0039	0.1165 ± 0.0016
n_s	1.01 ± 0.054	0.964 ± 0.026	0.967 ± 0.027	0.965 ± 0.024	0.9704 ± 0.0125	0.9599 ± 0.0045
h	0.721 ± 0.064	0.705 ± 0.041	0.697 ± 0.036	0.696 ± 0.028	0.729 ± 0.021	0.706 ± 0.008
τ_C	0.184 ± 0.094	0.117 ± 0.059	0.123 ± 0.061	0.110 ± 0.056	0.100 ± 0.020	0.106 ± 0.005
σ_8			0.871 ± 0.054	0.857 ± 0.059		
+ Running						
$\Omega_b h^2$	0.0241 ± 0.0023	0.0224 ± 0.00162	0.0221 ± 0.00130	0.0221 ± 0.00120	0.02289 ± 0.00074	0.02258 ± 0.00017
$\Omega_{cdm} h^2$	0.122 ± 0.0197	0.121 ± 0.0158	0.125 ± 0.0101	0.127 ± 0.0087	0.1113 ± 0.0070	0.1165 ± 0.0014
$n_s(k_n)$	0.968 ± 0.076	0.906 ± 0.0555	0.904 ± 0.0456	0.902 ± 0.0437	0.976 ± 0.0346	0.9595 ± 0.0038
$-dn_s/d\ln k$	0.077 ± 0.044	0.0847 ± 0.033	0.0736 ± 0.031	0.0697 ± 0.029	-0.0463 ± 0.025	0.0037 ± 0.005
h	0.760 ± 0.088	0.698 ± 0.075	0.677 ± 0.050	0.669 ± 0.039	0.7366 ± 0.0365	0.7061 ± 0.0068
τ_C	0.325 ± 0.129	0.248 ± 0.112	0.213 ± 0.0926	0.200 ± 0.0742	0.0984 ± 0.019	0.1083 ± 0.0062
σ_8			0.935 ± 0.066	0.936 ± 0.0710		

Note. The first four columns show the state as of Jan04. WMAP1 refers to the actual WMAP 1-year data, Jun03 is the compilation including the WMAP1 data and recalibrated Boomerang, CBI, VSA, and Acbar data, along with DASI and Maxima data. Means and standard deviations are given here. In all cases, the weak prior ($0.45 \le h \le 0.9$, age > 10 Gyr) is applied, and w_Q is fixed at minus of -1, the cosmological constant case. The curvature parameter Ω_k is fixed at zero. The LSS prior agrees with current weak lensing data and agrees with most of the cluster determinations. A weak redshift survey constraint is also imposed. The 2dF "prior" uses the stronger 2dF redshift survey results, but not a σ_8 prior. The primordial power spectrum index for scalar perturbations obeys $n_s(k) = n_s(k_n) + [dn_s/d\ln k(k_n)]\,(\ln k/k_n)$. For the first set of numbers $dn_s/d\ln k(k_n)$ is set to zero (no running of the spectral index). For the second set, it is allowed to vary. The last two columns show how the errors are expected to improve for WMAP with 4 years of data and Planck with 1 year of data, for the Fig. 9 simulations.

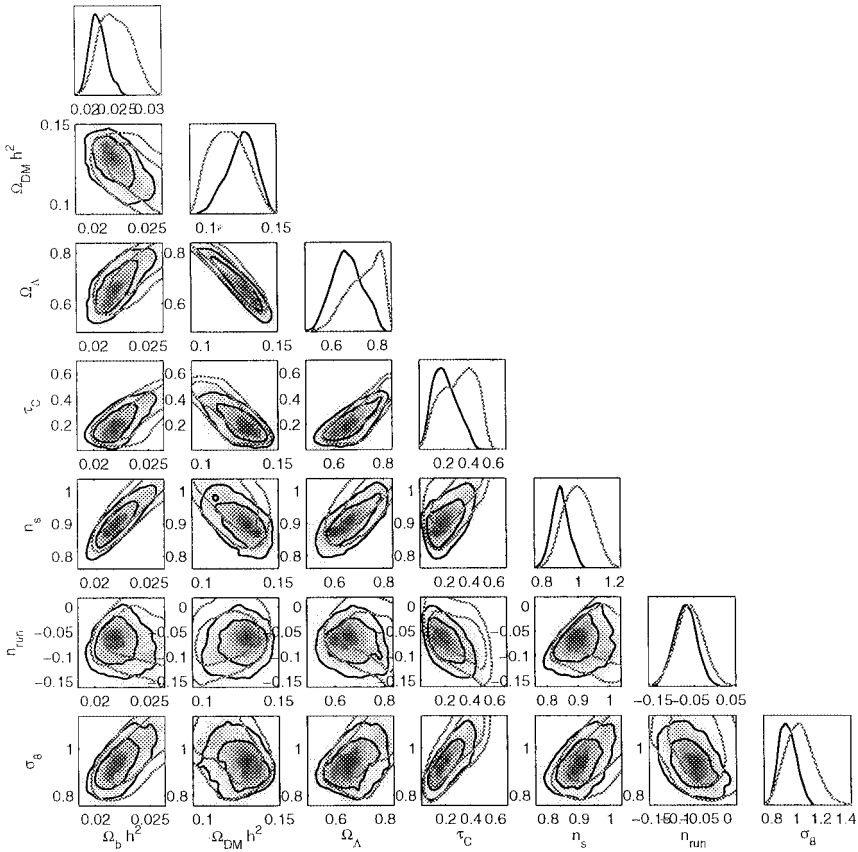

Fig. 7. Similar to Figure 6, except the scalar spectral index is allowed to run. Note the σ_8 and τ_C shifts indicated here and in Table I

Figure 7 and Table I address the level at which the WMAP1 and Jun03 CMB data would prefer a running spectral index $dn_s/d\ln k$ at about the two-sigma level. The projected distributions depend upon prior choices, e.g., Fig. 7 shows that if one restricts how large τ_C is allowed to be, $-dn_s/d\ln k$ would not be as large, accounting for the differences in the result here with those of the WMAP1 team's analysis (Spergel *et al.*, 2003). They highlighted how the non-CMB Lyman-alpha forest data in conjunction with the CMB suggested a running index. More effort is required to demonstrate that the forest estimates of power spectra are reliable enough to apply to this problem.

Of course in statistics one should just ignore two-sigma indications, and especially here when an extra cosmic parameter is added which has strong degeneracies with others in the basic minimal inflation mix. Figure 8 shows the conspiracy

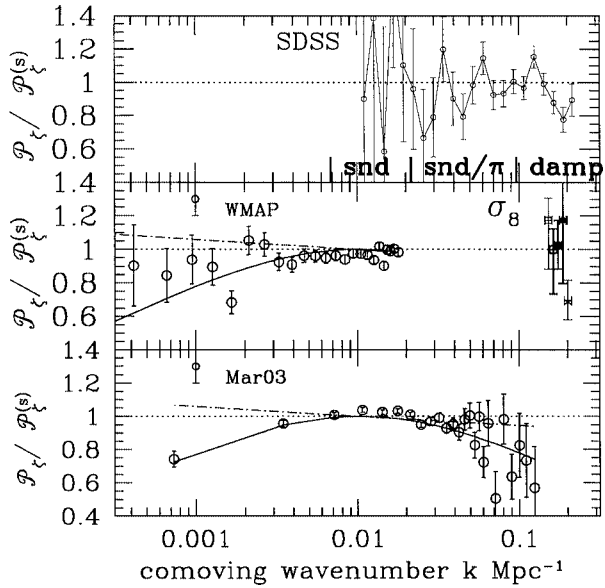

Fig. 8. The bottom panel translates the C_ℓ spectrum of Fig. 1 by mapping it from ℓ into (perpendicular) spatial wavenumber $k_\perp$, where $\ell \sim \mathcal{R}_{\rm dec} k_\perp$, and also dividing out the target spectrum. It indicates the ratio of primordial observed $\mathcal{P}_\zeta(k)$ to target $\mathcal{P}_\zeta^{(s)}$ in k-space with a window function for each band. The window spillover into neighbouring bands is not large, so it shows where the anomalies lie for the specific best-fit $n_{\rm s} = 0.957$ ΛCDM model. The downward bending curve is a shape that a running index of -0.09 would give. The low and high ℓ downward drive is evident. Breaking up the single low ℓ bandpower into many bandpowers as shown in the middle panel highlights the lower ℓ and $\ell \sim 20$ "anomalies." The right side of the middle panel shows σ_8^2, a broad-band power that probes cluster scales which reside near $k^{-1} \sim 4$ h^{-1} Mpc, relative to the target model. The solid square is derived from the Jun03 data, with $\sigma_8 \approx 0.85$. The heavy open square to its left is the current best value for weak lensing (Hoekstra and van Waerbeke, 2004, private communication), which has evolved slightly downward from the Jun03 estimate shown as the leftmost light square. Many X-ray cluster estimates are lower (rightmost light butterfly). The heavy butterfly to its immediate left is the σ_8 estimate from the SZ interpretation of the CBI, Acbar, BIMA high ℓ "anomaly" (e.g., Readhead *et al*. 2004). The top panel shows the recent SDSS data of Tegmark *et al*. (2004). Instead of dividing our Jun03 best-fit, which has some wiggles induced by the baryons, a best-fit wiggle-less "Γ-model" was used to highlight any obvious need, within the errors: the statistical answer is no (Tegmark *et al*., 2004). Galaxy biasing complicates the use of SDSS and 2dFRS, but there is no indication of any running index within these LSS datasets.

driving the indications of running index from the Jun03 data alone. The two low ℓ anomalies and the slightly lower power at high ℓ would prefer to bend the best-fit uniform acceleration model downward. By itself WMAP1 does this, and the addition of other experiments just takes this tendency and adds to it. However, BCP showed that the pre-WMAP1 Jan03 compilation of the data that included DMR and Archeops also had a distribution that preferred negative $[dn_s/d\ln k(k_n)]$, though with less statistical significance than the post-WMAP1 Mar03 set.

Because theorists like to theorize about low significance results in anticipation they might eventually emerge at high significance, much renewed discussion and many papers have now been written on whether the low ℓ anomalies or the combination of low and high ℓ anomalies indicate new physics. Within the context of inflation models, this involves arranging for q to change. If only low ℓ is the target, a scale is built associated with a target k, e.g., Bridle *et al.* (2003), Contaldi *et al.* (2003). Topology is another mechanism, building in a characteristic horizon-scale to discretize k-space, with just enough inflation to make the Universe just so big but no bigger. Trying to solve the high and low ℓ anomalies with the same mechanism utilizes the running index, or would need to build in a mix of scales.

Given this baroqueness, it is useful to explore the sensitivity of the running index distributions to cuts in the data. For example, Bridle *et al.* (2003) found $[dn_s/d\ln k(k_n)]$ of -0.04 ± 0.03 using all multipoles of WMAP1, the Jun02 versions of CBI and VSA and the Jan03 version of ACBAR, along with 2dF. When they excluded $\ell < 5$ from WMAP1, this dropped to -0.015 ± 0.03. To test this sensitivity further, we have marginalized over the $\ell = 2, 3, 4, 21, 22, 33$ multipoles of the WMAP1 data, which have "anomalous" bandpowers. We find -0.062 ± 0.043 compared with -0.088 ± 0.041 with no such cuts. Just removing $\ell = 22$ gives -0.082 ± 0.042. For this exercise, we did not constrain the running index by any cosmological broadended τ_C distribution, as reflected in Table.

Of course there should be a reason to justify removing or cleaning anomalies, e.g., that a source of systematic error is found or foregrounds and other residuals contaminate. In spite of much debate, there is no evidence that the low ℓs are low because of foreground contamination. However, when the quadrupole, octupole, etc., are obtained, the influence of the foregrounds should be reflected in the error bars. Slosar *et al.* (2004) improved the determination of errors on WMAP1 at low ℓ by marginalizing over foregrounds rather than using template subtractions. This leads to more power at low ℓ and better error determination. They improved the treatment of likelihood tails at low-ℓ over the standard WMAP1 prescription of Spergel *et al.* (2003), which was also used to get the results given in our figures and tables. Both effects decrease the statistical desire for a downturn and Slosar *et al.* find that the $\sim$2-σ effect drops to a $\sim$1-σ effect.

Our conclusion, as in Bridle *et al.* (2003), BCP, Readhead *et al.* (2004), and Slosar *et al.* (2004), is that evidence for a running index in the CMB data is not compelling. To get the large values allowed by the data would require rather dramatic changes in the acceleration of the universe over what is actually quite

Table II. Forecasted Cosmological Parameter Values and Their One-Sigma Errors for the Cases of Fig. 10 Contrast What May be Achievable for WMAP4, Planck1, and for future ground-Based Data (labeled ACT/SPT)

	Input	WMAP4	Planck1	WMAP4 + ACT/SPT-like
Flat				
$\Omega_b h^2$	0.02240	0.02311 ± 0.00051	0.02243 ± 0.00015	0.02291 ± 0.00025
$\Omega_{cdm} h^2$	0.1180	0.1077 ± 0.0049	0.1181 ± 0.0014	0.1105 ± 0.0035
n_s	0.9570	0.9738 ± 0.0137	0.9567 ± 0.0037	0.9716 ± 0.0080
τ_C	0.1080	0.1274 ± 0.023	0.106 ± 0.005	0.1270 ± 0.021
+ Running				
$\Omega_b h^2$	0.02240	0.02194 ± 0.00081	0.02236 ± 0.00017	0.02289 ± 0.00025
$\Omega_{cdm} h^2$	0.1180	0.1205 ± 0.0085	0.1166 ± 0.0015	0.1100 ± 0.0040
$n_s(k_n)$	0.9570	0.9014 ± 0.0415	0.9569 ± 0.0038	0.9727 ± 0.0090
$-dn_s/d\ln k(k_n)$	0	-0.0555 ± 0.030	-0.0044 ± 0.0052	0.0025 ± 0.0092
τ_C	0.1080	0.1436 ± 0.024	0.1074 ± 0.0056	0.1246 ± 0.0229
+ BSI				
$\Omega_b h^2$	0.02240	0.02974 ± 0.00196	0.02223 ± 0.00022	0.02266 ± 0.00042
$\Omega_{cdm} h^2$	0.1180	0.1059 ± 0.0168	0.1192 ± 0.0020	0.1067 ± 0.0057
n_s	0.9570	1.183 ± 0.074	0.9709 ± 0.0146	0.9688 ± 0.0388
τ_C	0.1080	0.2034 ± 0.030	0.1123 ± 0.0051	0.1602 ± 0.0266

Notes. The last column combines a polarization-sensitive bolometer-array ACT/SPT-like telescope (experimental choices as in Fig. 10) with WMAP4. Increasing the assumed coverage beyond the adopted 2.4% of the sky would increase precision in these idealized forecasts. For WMAP4 and Planck1, the quadrupole was included and the useful sky coverage was chosen to be unity. When the quadrupole is excluded, the sky coverage is dropped to 90%, ω_{mv} and $\mathcal{P}_{GW}/\mathcal{P}_\zeta$ are added to the parameter mix, and a tensor component and weak lensing effects on the power spectra are included in the target model, the errors grow modestly, usually within 20% of the sigmas listed. Of the 9 parameters, WMAP4 would determine 3 orthogonal combinations to ± 0.01, 7 to ± 0.1; with an SPT/ACT-like experiment, these rise to 4 and 8; and for Planck1, to 6 and 8. The lower rows illustrate the impact of including many more parameters to characterize $n_s(k)$ than the two in the running index model. Here 24 parameters defining the amplitudes of $\mathcal{P}_\zeta(k)$ in 24 bands are added to the standard mix. The impact is not as severe as one might have expected since the polarization information breaks this severe degeneracy because the peaks and dips of $C_\ell^{(EE)}$ and $C_\ell^{(TE)}$ are in different locales than $C_\ell^{(TT)}$. In Souradeep *et al*. (1998), it was shown that parameter determination was significantly degraded if there was no polarization information when similar numbers of $\mathcal{P}_\zeta(k)$ bands were added.

a narrow range on the inflaton potential surface, manifested in a soft or even a radical breaking because of changing braking.

3.2. Forecasts of Parameter Precision

The running index issue will probably be with us for quite a while, but forecasts are rosy for how well planned CMB experiments can answer this question: if there is a running index, it will be detected in the next generation of experiments, and if there is not it will be strongly constrained. This is illustrated in Fig. 10, Table II as well as in Fig. 9 and Table I.

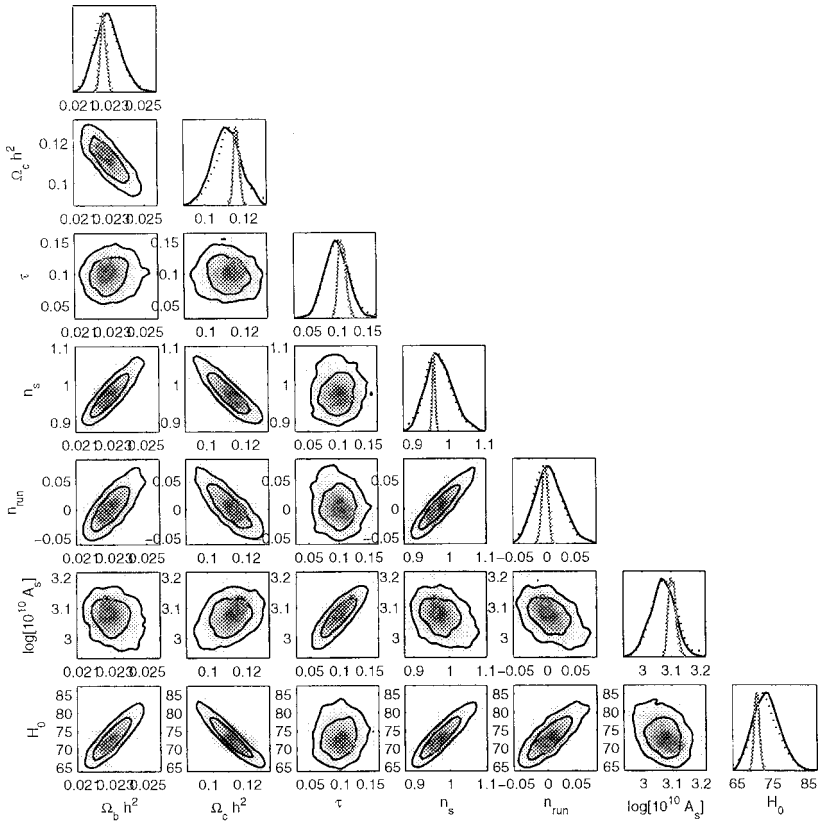

Fig. 9. Forecast of one- and two-sigma contour regions for WMAP4 (black outer contours, light blue shading) and Planck1 (red inner contours) show how the errors of Fig. 7 may improve in the future. Note that some of the variable shown differ from those in Fig. 7 and there are changes in axes scales. Estimations were on simulated datasets generated using the no-running-index best-fit to the Jun03 CMB data. Only the 94 GHz channels were used for the 4-year simulation of WMAP4 and only the 150 GHz channels for the 1-year simulation of Planck1 in these forecasts. No LSS priors were imposed. Table I gives means and errors for these two cases. The precision sharpens when all channels are brought to bear. Further, both Planck and WMAP are expected to observe for roughly double these periods, decreasing the noise component of the bandpower errors, with the sample-variance (cosmic-variance) component unaffected. One may therefore interpret these as conservative estimates, but the forecasts here do not include all of the extra complications associated with foreground separation. As Fig. 10 shows, anticipated ground-based experiments beyond the ones used in Fig. 7 will also have a powerful sharpening effect on precision.

The precision for ground + WMAP4 would improve with larger sky coverage. For the numbers in the table, it was assumed that the primary spectrum beyond 2000 would be contaminated by secondary signals, but component separation should mitigate this, and the parameters are not sensitive to lesser cutting. Note

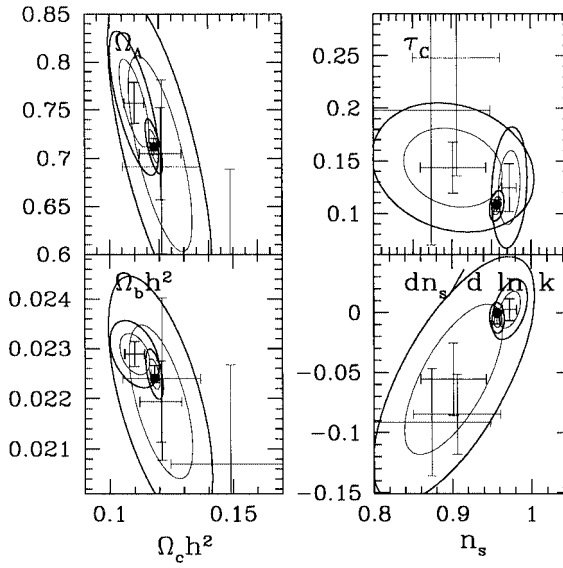

Fig. 10. The forecasts of WMAP4 (green), Planck1 (blue), and WMAP4 + groundbased ACT/SPT-like data (red) are shown compared with the target value (black dot). Projected one-sigma error bars are shown, and the one- and two-sigma ellipses which illustrate the correlations. The (magenta) cross shows the precision of the Jun03 data when the scalar spectral index is allowed to run, as it is for the simulations as well. The bigger (cyan) cross shows the state with the pre-WMAP Jan03 data. Large dedicated groundbased telescopes targeting high ℓ with huge arrays of bolometers (e.g., ACT and SPT) or of HEMTs (QUIET), when combined with WMAP, should greatly increase parameter precision in the leadup to Planck. For this simulation, ACT/SPT experimental parameters were adopted, and the bolometers were assumed to be polarization sensitive to show their powerful impact on EE mode detection. The assumed coverage was 2.4% of the sky, 1000 sq degrees. Increasing this would further improve the parameter estimates given in Table II since errors on many bands are sample-variance limited. Planck does so well because of its all-sky coverage, and will have a large impact on constraining multiparameter deviations from the simple uniform-acceleration inflation models.

how the larger baseline in ℓ significantly decreases the degeneracy and also the drift in the value of the running index one would estimate from the data relative to the target value.

For the forecasts of Table II, power spectra and their errors in Figures 3, 4, 5 were calculated using "faster-like" algorithms of the sort we have applied to Boomerang. The idealizations make it "superfast." The cosmic parameter errors

were estimated using Fisher or curvature matrices about maximum-likelihood values, rather than using Monte Carlo Markov Chains on the simulated data as in Table I. This means the parameters are treated as completely internal rather than completely external, as in MCMC. (See BCP for a discussion of the difference; the fixed grid approach was a hybrid, with amplitudes and experimental variables treated as internal, the rest external.) For both forecasting methods, the same Jun03 best-fit model with zero-running index was used and the experimental parameters were essentially the same. The maximum-likelihood drifts from the listed input cosmic parameter values of the target model depend upon the specific realization. Note that the errors of the Fisher-based forecast given here are quite similar to the MCMC values given in the last two columns of Table I.

Thus the superfast forecasts have been nicely validated by comparison with the MCMC results. They also give results compatible with what was actually obtained with Boomerang and WMAP when the real experimental specs were used. The forecasts can be made more sophisticated with some attempts at addition of foregrounds and residual signals and subsequent removal by parameterized "power spectrum cleaning." Tegmark *et al.* (2000) explored many aspects of the impact foreground contamination could have on forecasted cosmological parameter errors. Increasingly sophisticated forecasts can still only be considered as partial steps towards the full mocks of a given experiment that one actually needs.

Forecasting has a long history in the CMB, as a necessary ingredient for experimental proposals, and for showing feasibility of measuring new theoretical effects. Many realizations, experimental configurations, and theoretical assumptions can be checked very quickly. This leads to an overwhelming amount of information on the stages we expect to see between the data now and the Planck results, because there are so many polarization-sensitive ground-based experiments in various configurations either funded or proposed. Further there are many theoretical parameters that can be added to further add to the information glut, yet turning them all on at the same time obscures what will happen in practice.

In this paper, we have chosen to highlight only three forecasting cases, WMAP4, Planck, and a fiducial high resolution ground-based experiment of modest sky coverage compared with what is possible. This reflects our experience that erring on the conservative side may reflect the real issue, which is how complex the analysis of the actual polarization data will turn out to be, and how much it will limit the precision we can obtain from the ground; and indeed from space. For polarization-targeting ground experiments, we can look forward to a wonderful set of developments. Listing some of the cases that have been considered gives an idea of the range.

Apart from WMAP4 and Planck1 with one channel, we have considered the following: WMAP2, WMAP4, WMAP8, using all five channels as well as the W channel with its $13'$ resolution adopted here, usually assuming 0.9 for $f_{\rm sky}$, detector noise, and beam sizes courtesy of Lyman Page. Planck1 and Planck2, using either the 143 GHz channel with beam $7'$ alone, or with the 220 GHz, $5'$ and

100 GHz, 9′ polarization-sensitive bolometers (PSBs), or μ together with the lower frequency HEMTs (Planck "blue book" numbers, augmented by the most recent PSB numbers from Andrew Lange). With everything included forecasted errors do improve somewhat, but are often largely sample variance limited.

We have considered forecasts for the Boomerang 2003 flight (although the polarization analysis of the real data is heavily underway), and for Acbar (continuing to observe, specs for current and subsequent observing seasons from John Ruhl).

For the South Pole-based BICEP, using PSBs at 143 GHz, 40′ and 100 GHz, 60′ observing 1000 sq deg in 260 days, numbers from Lange and Eric Hivon, with similar capabilities suggested for an experiment at another Antarctic site, Dome C, courtesy of de Bernardis. For QUaD (Quest mounted on DASI at the South Pole), using PSBs at 143 GHz, 4.0′ and 100 GHz, 6.3′ observing 200 sq deg in 260 days, specs from Lange and Hivon, with similar numbers in a separate Cardiff-based proposal. Prospects for BICEP and QUaD are very good for polarization and both are expected to be observing in 2005. See Bowden *et al*. (2004) for a full discussion of optimizing ground-based CMB polarization experiments, in terms of the tradeoff of sky coverage and sensitivity per pixel.

The proposed QUIET experiment from Princeton, Chicago, JPL/Caltech, using new HEMT-MMIC array technology under development at JPL, would be mounted on the CBI platform in Chile, with large beams, 44 and 90 GHz, 42′, over 2000 and 8000 sq deg, and small beams, 44 and 90 GHz, 4′, over 2000 and 8000 sq deg, Forecasts look very good for polorization and the first phase could begin in late 2005. The South Pole Telescope numbers used only 220 GHz, 1.3′, the SZ null channels and were from John Ruhl. We assumed a noise for polarization $\sqrt{2}$ times that in total anisotropy per pixel. For the Chile-based ACT, the beam is slightly larger than for the SPT. A deep mode of 100 sq deg was considered in addition to the 1000 sq deg we chose to highlight here—sensitivities from Lyman Page. In contrast to Fig. this showed the power in the lesing-induced B-Mode could in principle be detected. A fiducial CMBPol and an essentially cosmic variance limited all-sky survey at SPT/ACT resolution with very tiny noise have also been considered, Needless to say, for the latter the target parameters are recovered at the best-you-can-do level.

We now turn back to the results shown in Table II. The last set of rows show how the error bars open up when searching for more radical braking than the running index model gives. Consider the case when $\mathcal{P}_\zeta(k)$ has a structure of unknown shape, as in radical broken scale invariance (BSI). For two given cosmological parameter sets, a $\mathcal{P}_\zeta(k)$ could be fashioned to morph one $\mathcal{C}_\ell^{(\mathrm{TT})}$ into another. (see e.g. Souradeep *et al*. (1998), Wang *et al*. (1999) for a discussion of the role this degeneracy plays in parameter degradation). Polarization information breaks this severe degeneracy because the peaks and dips of $\mathcal{C}_\ell^{(\mathrm{EE})}$ and $\mathcal{C}_\ell^{(\mathrm{TE})}$ are in different locales. Parameterization is in terms of power amplitudes in a number k-bands of proscribed shape. Twenty-four bands were chosen for the Table II case. Apart from

the conventional banding in $\Delta\mathcal{P}_\zeta$, we have expored the impact of band-colours (bands in Δn_s), continuous wavelets, among others. The colour-banding makes more of a difference. However, although the errors determined are somewhat sensitive to the primordial spectrum band-type, band-placing and band-number, polarization does indeed nicely mitigate the effect of BSI-induced degeneracy for these planned experiments. Non-CMB information from LSS also helps to break degeneracies between cosmic parameters and $\mathcal{P}_\zeta(k)$-structure. Having τ_C from the low ℓ is important for breaking parameter degeneracies.

As more parameters characterizing the inflation model are added, the precision continues to diminish unless near-degeneracies can be broken. For example, with a target value for $\mathcal{P}_{GW}/\mathcal{P}_\zeta$ of 0.17, the Planck1 realization of Fig. 4 shows a detection of the tensor B-mode is possible, which could lead to a good estimate of this amplitude. Getting the B-mode is very important for this the specific example, determining 8 other cosmological parameters as well, gave a 0.135 ± 0.028 detection. With somewhat more optimistic noise forecasts, but allowing for the incomplete sky coverage mixing of E and B modes, Lewis (2003) finds that Planck should be able to detect primordial tensor modes at 95% confidence with greater than 95% probability if $\mathcal{P}_{GW}/\mathcal{P}_\zeta \eta\, 0.03.$ has a 0.12 ± 0.03 detection. Getting the B-mode helps.

We can conclude from exercises such as these on the experiments coming that parameters characterizing GW signals, mildly broken scale invariance associated with a running index, subdominant isocurvature components, and even radically broken scale invariance can be determined within the CMB data.

REFERENCES

Bond, J. R. (1994). Testing inflation with the cosmic background radiation. In *Relativistic Cosmology*, M. Sasaki, ed., (Proceedings of the 8th Nishinomiya-Yukawa Memorial Symposium) Academic Press, New York. (astro-ph/9406075).

Bond. J. R. (1996). Theory and observations of the cosmic background radiation. In *Cosmology and Large Scale Structure* (Les Houches Session LX, August 1993) R. Schaeffer, ed., Elsevier Science, New York.

Bond, J. R., Contaldi, C. R., and Pogosyan, D. (2003). *Philosphical Transactions of the Royal Society of London A* **361**, 2435 (astro-ph/0310735).

Bond. J. R. and Crittenden, R. G. (2001). In *Proceedings of the NATO ASI, Structure Formation in the Universe*, R. G. Crittenden, and N. G. Turok, eds., Kluwer, Norwell, MA (astro-ph/0108204).

Bond. J. R., *et al*. (in press). *Astrophysics Journal* (astro-ph/0205386).

Bowden, M., *et al*. (2004). *Monthly Notices of the Royal Astronomical Society* **349**(1), 321–335 (astro-ph/0309610).

Bridle, S. L., Lewis, A. M., Weller, J., and Efstathiou, G. (2003). *Monthly Notices of the Royal Astronomical Society* **342**, L72 (astro-ph/0302306).

Contaldi, C. R., *et al*. (2003). *Journal of Cosmology and Astroparticle Physics* **0307**, 002, (astro-ph/0303636).

Dickinson, C., *et al*. (2004). *Monthly Notices of the Royal Astronomical Society* (astro-ph/0402498).

Goldstein, J. H., *et al*. (2003). *Astrophysics Journal* **599**, **773** (astro-ph/0212517).

Habib, S., Heitmann, K., Jungman, G., and Molina-Paris, C. (2002). *Phys. Rev. Lett.* **89**, 281301.
Hivon, E. and Kamionkowksi, M. (2002). *Science* **298**, 1349 (astro-ph/0211553).
Hu, W. (2000), *Physical Review D* **62**, 043007.
Kinney, W. H. (2002). *Physical Review D* **66**, 083508.
Kofman, L. A. and Linde, A. D. (1987). *Nuclear Physics B* **282**, 555.
Kofman, L. A. and Pogosyan, D.Yu. (1988). *Physics Letters B* **214**, 508.
Leach, S. M. and Liddle, A. R. (2003). *Physical Review D* **68**, 103503 (astro-ph/0306305).
Lidsey, J. E., *et al.* (1997). *Review of Modern Physics* **69**, 373.
Martin, J. and Schwarz, D. J. (2003). *Physical Review D* **67** 083512 (astro-ph/0210090).
Page, L., *et al.* (2003). *Astrophysics Journal* (Suppl.) **148**, 233.
Peiris, H. V., *et al.* (2003). *Astrophysics Journal* (Suppl.) **148**, 213.
Readhead, A. C. S., *et al.* (2004). *Astrophysics Journal* **609**, 408, (astro-ph/0402359).
Salopek, D. S., Bond, J. R., and Bardeen, J. M. (1989). *Physical Review D* **40**, 1753.
Salopek, D. S. and Bond, J. R. (1990). *Physical Review D* **42**, 3936.
Salopek, D. S. and Bond, J. R. (1991). *Physical Review D* **43**, 1005.
Schwarz, D. J., Terrero-Escalante, C. A., and Garcia, A. A. (2001). *Physics Letters B* **517**, 243–249.
Spergel, D. N., *et al.* (2003). *Astrophysics Journal* (Suppl.) **148**, 175.
Slosar, A., Seljak, U., and Makarov, A. (2004). *Physical Review D* **69**, 123003, (astro-ph/0403073).
Souradeep, T., Bond, J. R., Knox, L., Efstathiou, G., and Turner, M. S. (1998). Prospects for measuring inflation parameters with the CMB. *In proceeding for COSMO-97*, Ambleside, UK, Sept. 1997, ed. L. Roszkowski (World Scientific), (astro-ph/9802262).
Tegmark, M., Eisenstein, D. J., Hu, W., de Olivera-Costa, A. (2000). *Astrophysics Journal* **530**, 133.
Tegmark, M., *et al.* (2004). *Astrophysics Journal* **606**, 702. (astro-ph/0310725).
Wang, L., Mukhanov, V. F., and Steinhardt, P. J. (1997). *Physics Letters B* **414**, 18–27 (astro-ph/9709032).
Wang, Y., Spergel, D. N., and Strauss, M. A. (1999). *Astrophysics Journal* **510**, 20.